

## Scrape-off layer intermittency in the Castor tokamak

M. V. A. P. Heller, Z. A. Brasilio, I. L. Caldas, J. Stöckel, and J. Petrzilka

Citation: *Phys. Plasmas* **6**, 846 (1999); doi: 10.1063/1.873324

View online: <http://dx.doi.org/10.1063/1.873324>

View Table of Contents: <http://pop.aip.org/resource/1/PHPAEN/v6/i3>

Published by the [American Institute of Physics](#).

---

### Related Articles

Merging of high speed argon plasma jets

*Phys. Plasmas* **20**, 012704 (2013)

Design and validation of the ball-pen probe for measurements in a low-temperature magnetized plasma

*Rev. Sci. Instrum.* **84**, 013505 (2013)

Effect of multiple scattering on Cerenkov radiation from energetic electrons

*Phys. Plasmas* **20**, 013302 (2013)

Current density distributions and sputter marks in electron cyclotron resonance ion sources

*Rev. Sci. Instrum.* **84**, 013303 (2013)

Radio frequency current-voltage probe for impedance and power measurements in multi-frequency unmatched loads

*Rev. Sci. Instrum.* **84**, 015001 (2013)

---

### Additional information on Phys. Plasmas

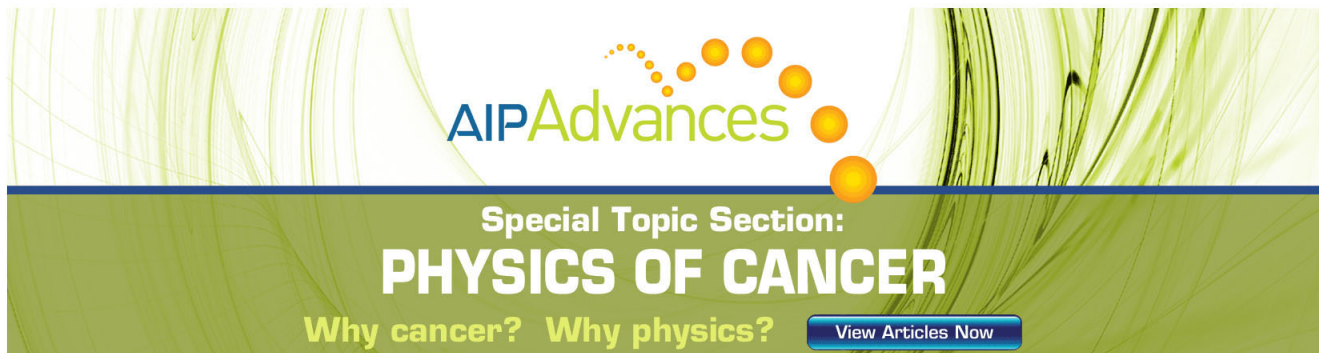
Journal Homepage: <http://pop.aip.org/>

Journal Information: [http://pop.aip.org/about/about\\_the\\_journal](http://pop.aip.org/about/about_the_journal)

Top downloads: [http://pop.aip.org/features/most\\_downloaded](http://pop.aip.org/features/most_downloaded)

Information for Authors: <http://pop.aip.org/authors>

## ADVERTISEMENT



**AIP Advances**

Special Topic Section:  
**PHYSICS OF CANCER**

Why cancer? Why physics? [View Articles Now](#)

# Scrape-off layer intermittency in the Castor tokamak

M. V. A. P. Heller, Z. A. Brasilio, and I. L. Caldas

*Institute of Physics, University of São Paulo, C. P. 66318, 05315-970 São Paulo, SP, Brazil*

J. Stöckel

*Institute of Plasma Physics, Prague, Czech Republic*

J. Petrzilka

*Faculty of Mathematics and Physics, Charles University, Prague, Czech Republic*

(Received 10 August 1998; accepted 23 November 1998)

Spatial-temporal intermittency of floating potential and ion saturation current fluctuations is analyzed by using data obtained from two probes arrays in the scrape-off layer of the CASTOR tokamak [*Proceedings of the 1996 International Conference on Plasma Physics* (Nagoya) (International Atomic Energy Agency, Vienna, 1997), Vol. I, p. 322]. For these ion saturation current fluctuations with non-Gaussian probability density functions, a conditional averaging analysis shows coherent structures with correlation lengths and lifetimes larger for larger amplitude conditions. Nevertheless, there is no evidence of such large structures in the potential fluctuations. Furthermore, wavelet transforms are used to analyze these nonstationary fluctuations and obtain details not observed with the Fourier technique. So, examining wavelet power and coherence spectra, strong intermittency is found for both kinds of fluctuations, in a time scale two orders of magnitude higher than that observed in the conditional analysis. Moreover, during the discharges the observed wavelet quadratic coupling alters intermittently for some low-frequency components. © 1999 American Institute of Physics. [S1070-664X(99)00803-4]

## I. INTRODUCTION

One of the main technological problems in the operation of tokamaks is the power density deposited at the limiter and inner wall, with the release of neutrals by sputtering due to localized heat and particle loadings. The consequent increase of impurity content in the plasma core degrades the plasma confinement conditions. Thus, the application of tokamaks as nuclear fusion reactors requires the control of this power deposition. On the other hand, this deposition depends on the width of the scrape-off layer (SOL), formed around the plasma, which is altered by the electrostatic turbulence characteristics in this region.<sup>1,2</sup> Therefore, controlling turbulence at the SOL could reduce the power density deposited at the limiter and inner wall, improving plasma confinement in tokamaks. So, understanding turbulence in this region may lead to the development of appropriate control methods to avoid this problem.

However, despite the recent experimental effort, turbulence in the SOL has not been completely characterized yet.<sup>1,2</sup> Thus, one of the most investigated features is the existence of coherent structures in this region, which would affect the plasma transport and modify the turbulence description.<sup>3,4</sup> Nevertheless, up to now the existence of coherent structures in SOL has not been clearly confirmed.<sup>5</sup>

In this work, we applied some advanced numerical techniques to search coherent structures and intermittency in the turbulent electrostatic fluctuations observed at the CASTOR tokamak scrape-off layer.<sup>6</sup>

Probability density functions (PDF) of these data showed deviations from the Gaussian distribution, i.e., the analyzed fluctuations are not randomly distributed in space

and time. These non-Gaussian features suggested the existence of intermittency with formation and destruction of coherent structures. So, we applied complementary numerical techniques to obtain information about intermittency, coherent structures, and their nonlinear interactions.

To verify the existence of coherent components, we used a conditional averaging technique that follows the statistical evolution of selected conditions in the measured fluctuations.<sup>7</sup> Thus, we found coherent components with correlation lengths and lifetimes larger for larger fluctuation level conditions.

Besides this conditional technique, we also used wavelet analysis to detect the intermittency by resolving short-lived events during the considered plasma discharges, and to follow in time the contribution of the various frequencies to the analyzed signal. For that we computed wavelet transforms and, by using definitions analogous to the usual definitions of Fourier analysis, we obtained wavelet cross-spectra and cross-coherence. Thus, we obtained local information about intermittent correlation at a particular frequency band and temporal location in the time-scale plane.<sup>8</sup> In the literature these quantities are related to particle transport to identify the dominant drive source of particle flux at the scrape-off layer.<sup>1</sup> So, we estimated the driven turbulence particle flux that varies intermittently by an order of magnitude during the discharge time.

On the other hand, when a signal has a spatial structure of any kind, it is expected that some phase coupling occurs.<sup>9-11</sup> Then, to measure the amount of phase coupling present in a signal or between two signals, we calculated bicoherence spectra with wavelet analysis as it is computed

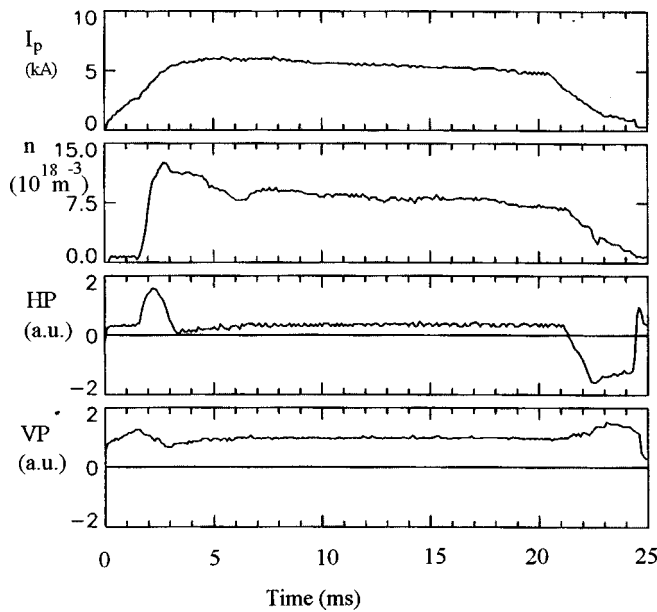


FIG. 1. Tokamak time profiles for the studied discharge: plasma current, density, horizontal and vertical position of the plasma column, from top to bottom.

with Fourier analysis.<sup>12</sup> This wavelet bicoherence detects phase coupling between short lived wavelets rather than between modes as Fourier bicoherence. As predicted by this technique, we observed phase coupling for two frequencies present in a signal along with their sum or difference frequencies.

Thus, in this work, by applying the mentioned advanced numerical techniques, we report episodes of coherent structures and intermittency in the analyzed turbulent electrostatic fluctuations observed at the CASTOR tokamak scrape-off layer.<sup>6</sup>

We analyzed data measured by two arrays of probes (ten tips spaced poloidally by  $d=0.005$  m), which are spaced toroidally by 0.010 m. The first array measures the ion saturation current ( $\bar{I}_{\text{sat}}$ ) and the second one measures the floating potential ( $\bar{\varphi}$ ).<sup>6,13</sup> Neglecting temperature fluctuations, the probes measure the plasma potential,  $\bar{\varphi}_p$ , and the electron density,  $\bar{n}_e$ .

The main plasma parameters in this experiment are major radius  $R_0=0.40$  m, minor radius (limiter position)  $a=0.085$  m, toroidal magnetic field  $B_t=1.0$  T, plasma current  $I_p=6$  kA, pulse length of 25 msec, and safety factor at the limiter  $q(a)\approx 15$ . Radial profiles of the floating potential and electrical current fluctuations show plateaux indicating a last closed magnetic surface at  $r\approx 0.083$  m, just 0.002 m from the limiter. Figure 1 shows typical time profiles of the discharge studied in this paper. These profiles are stationary in the interval  $5 \text{ msec} < t < 20 \text{ msec}$ , for which the fluctuations are analyzed.

To analyze turbulence, we considered simultaneous two-point measurements of electrostatic quantities at the scrape-off layer (at  $r=0.090$  m, 0.005 m from the limiter and 0.020 m from the vessel).<sup>6</sup> The ratios of the magnitude of fluctuations to their mean values in the region of measurements are approximately 0.20.

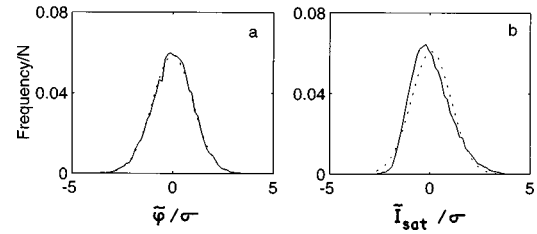


FIG. 2. Probability distribution functions for floating potential fluctuations (a) and ion saturation current fluctuations (b) as a function of fluctuation amplitude normalized to the respective standard deviation. Dashed curves represent Gaussian functions.

Signals from the diagnostics were sampled at a rate of 308 kHz. Calculations are done on the samples after high-pass digital filtering with a cutoff frequency of 1.5 kHz. The frequency spectra are broad, up to a few 5 to 80 kHz, with decreasing power density toward high frequencies. On the equatorial plane fluctuations present long wavelengths, typically  $\lambda_\varphi/a\approx 0.9$  and  $\lambda_n/a\approx 0.6$ . The order of magnitude of the particle flux in the SOL induced by turbulence was estimated as  $1 \times 10^{19} \text{ m}^{-2} \text{ s}^{-1}$ .

Average dispersions are linear (i.e., the average poloidal wave vectors,  $\bar{k}$ , are proportional to the frequencies), in the region of high spectral power density and  $\sigma_k/\bar{k} > 1$ . The product  $\bar{k}\rho_s \approx 1$  (where  $\rho_s$  is the ion gyroradius) is ten times higher than that expected from drift wave theories,<sup>1</sup> but similar to values obtained in other tokamaks.

Magnetohydrodynamic (MHD) spectra for fluctuating radial magnetic field show a coherent peak at the frequency of 50 kHz (Ref. 6) for which the electrostatic power density is low. Therefore, MHD is not the driving mechanism of the electrostatic turbulence analyzed in this work. Moreover, experimental correlations between these two kinds of oscillations are usually low.<sup>1</sup>

In Sec. II we present a short description of the conditional analysis with the results obtained with our data. In Secs. III and IV we present linear and bicoherence wavelets that are appropriate to analyze the nonstationary behavior of our signals. Finally, in Sec. V some conclusions are drawn for electrostatic fluctuations.

## II. CONDITIONAL ANALYSIS

The usual approaches to characterize plasma turbulence in tokamaks assume that fluctuating fields are randomly distributed in space and time.<sup>14</sup> This assumption of homogeneity can be examined with the probability density functions (PDF) and their moments. In fact, Gaussian signals have known higher-order moments, such as skewness ( $S=0$ ) and kurtosis ( $K=3$ ), and these moments can be calculated from the analyzed data.

Figure 2 shows PDF for floating potential fluctuations ( $S=0.04 \pm 0.02$ ,  $K=3.07 \pm 0.04$ ) and ion saturation current fluctuations ( $S=0.66 \pm 0.02$ ,  $K=3.40 \pm 0.04$ ). In our data only the ion saturation current fluctuations deviate from Gaussian distribution significantly. Similar values were obtained with all probes of the two arrays.

These non-Gaussian features imply the formation and destruction of long-scale length coherent structures.<sup>15</sup> To obtain information about these structures, we investigated this turbulence with conditional statistical analysis that shows the dependence of the statistical characteristics of the fluctuations on the amplitude of the measured parameter. Moreover, this analysis applies a conditional averaging technique to separate the coherent structures from the incoherent turbulence.

The conditional time average,  $\Phi(x+d, \tau)$ , is an estimate of the time average of  $\Phi$  at some distance,  $d$ , and time shifted,  $\tau$ , away from a reference point at the position  $r$ , when the oscillation at the reference point takes a value  $\Phi = \Phi_c$  during a time sequence  $t_j$ :

$$\Phi_{\text{cond}}(x+d, \tau) = (1/N) \sum_{j=1}^N \Phi_j(x+d, \tau, t_j, \Phi_c). \quad (1)$$

Following Ref. 7, we approximate this average by a power series representation around the condition  $\Phi_c$ , applied to the signal at the reference point  $r$ :

$$\Phi'_{\text{cond}}(x+d, \tau) = \sum_{i=1}^N \alpha_i(d, \tau) [\Phi_c]^i. \quad (2)$$

The coefficients  $\alpha_i$  do not depend on the condition being imposed on the signal, but only on the separation,  $d$ , and the time delay,  $\tau$ . We utilize only the first three coefficients in Eq. (2) to estimate the conditional averages. These coefficients are evaluated by minimizing the mean square error  $\delta$ :

$$\delta = \langle [\Phi'_{\text{cond}}(x+d, \tau) - \Phi_{\text{cond}}(x+d, \tau)]^2 \rangle. \quad (3)$$

To apply this algorithm, we used data from a reference and four other probes in the same radial position ( $r/a = 1.06$ ) equally spaced ( $d = 0.51$  cm) in the poloidal direction, choosing  $\Phi_c$  as a value of  $\Phi$  at  $(x=0, t)$  measured with the reference probe in the equatorial plane, and  $x = nd$  ( $n = 1, 2, 3, 4$ ) as the positions of the other four probes.

For the conditional average to track a coherent component in a signal, the condition imposed must define the structure, that is, the structure should be defined by its amplitude. Also the structure must be strongly coherent along the defined trajectory (in our experiment the trajectory is assumed along the poloidal direction), and the shape of the structure must not change. If these conditions do not exist, the conditional average will have the effect of "smearing out" the shape of the coherent components and no structure is detectable.

In Figs. 3(a) and 3(b) we compare the conditional averages (dashed lines),  $\Phi'_{\text{cond}}$ , and cross-correlation functions (continuous lines),  $R$ , for ion saturation fluctuations. Here  $R$  is plotted for reference purposes since it reveals only the Gaussian component of the considered fluctuating quantity. In these figures, each set of five curves corresponds to the conditional averages calculated with data from the reference and the other four probes at different poloidal separations, for the conditions  $\Phi_c = 1\sigma$  [Fig. 3(a)] and  $\Phi_c = 3\sigma$  [Fig. 3(b)] (where  $\sigma$  is the fluctuation standard deviation). The conditional averages are normalized such that  $\Phi'_{\text{cond}}(x, \tau = 0)/\Phi_c = R$ . For these fluctuations the conditional averages

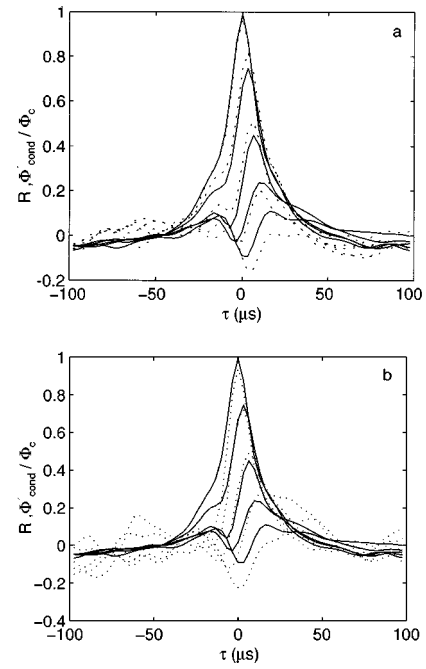


FIG. 3. Normalized cross-correlation functions  $R$  (—) and conditional averages  $\Phi'_{\text{cond}}$  (---) for ion saturation fluctuations for the condition  $\Phi_c = 1\sigma$  (a); the same for the condition  $\Phi_c = 3\sigma$  (b).

differ from the cross-correlation functions, especially for  $\Phi_c = 3\sigma$ . For floating potential fluctuations the shape of the conditional averages closely resembles the cross-correlation functions.

Figure 4 shows the conditional average for ion saturation fluctuations for the same condition of Fig. 3(a) calculated for different poloidal separations at the same radial position. The curves are shifted on the vertical axis by the poloidal probe separation. The shift of the peaks in time as a function of probe separation permits us to obtain the poloidal phase velocity of the waves in the plasma.

At a distance  $d \approx 1.5$  cm away from the reference probe, the conditional averages develop a peak with negative amplitude, which is phase delayed with the positive peak (positive peak defines the phase velocity). Furthermore, as the distance between probes increases, the phase-shifted component become more significant, indicating propagation in a medium with frequency and wave number related dispersion properties. The peaks of the conditionally averaged fluctua-

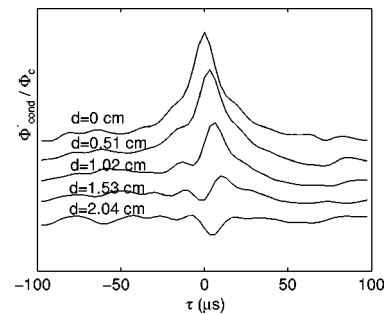


FIG. 4. Normalized conditional averages for the same fluctuations and conditions of Fig. 3(a) for different poloidal separations  $d$ .

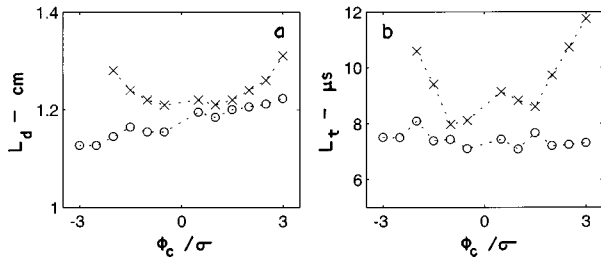


FIG. 5. Exponential decay coefficients in space,  $L_d$  (a), and time,  $L_t$  (b), for different conditions,  $\Phi_c$ , for floating potential (O) and ion saturation current (X) fluctuations.

tions were tracked against the poloidal separation and against the corresponding time shift. The exponential decay coefficients  $\beta_d$  and  $\beta_\tau$  were calculated by fitting exponential curves to the experimental data. Exponential space and time decay coefficients were calculated for several conditions  $\Phi_c$  imposed to data.

A conditional correlation length,  $L_d = \beta_d^{-1}$ , and lifetime,  $L_t = \beta_\tau^{-1}$ , were obtained for both fluctuations from the decay coefficients. Figure 5 shows correlation lengths,  $L_d$ , for specified conditions at (a)  $r = 9$  cm and (b) lifetimes,  $L_t$ . The changes in correlation lengths and lifetimes for different conditions for potential fluctuations are less than 7%. For ion saturation fluctuations the variation in  $L_d$  for different conditions is  $\approx 8\%$ . The change in  $L_t$  is  $\approx 32\%$ . We calculated the error of these variations as 2% since the estimated correlation lengths and lifetimes errors were of 1%. These precisions are enough to identify a significant asymmetry between positive and negative conditions (Fig. 5). Larger correlation lengths and lifetimes occur at larger conditions. This result seems consistent with the hypothesis that structures at larger amplitudes have longer lifetimes compared with structures with a smaller condition.

### III. SPECTRAL WAVELET ANALYSIS

Wavelet analysis completes the Fourier analysis and permits often a similar interpretation, but amplifies it, by adding time resolution. Therefore, this numerical technique is adequate to analyze our signals with rapidly changing frequencies during short intervals.<sup>8,11,16,17</sup>

The application of the wavelet method on our nonstationary signal analysis is based on a wavelet function set that changes its size and position by dilatation and shifting. Thus wavelet transform decomposes the experimental time series using a wavelet basis of functions localized both in time and frequency domains. However, a good frequency resolution can only be achieved by means of a large sampling window, which results in a poor time resolution; on the contrary, a good time resolution implies short windows, which results in a poor frequency resolution.

In this analysis we used the continuous wavelet transform based on the Morlet wavelet:<sup>11</sup>

$$\Psi_a(t) = a^{-1/2} \exp[i2\pi t/a - (t/a)^2/2]. \quad (4)$$

A frequency  $f = 2\pi/a$  is assigned to each scale  $a$ . The frequency resolution of the wavelet  $\Psi_a(t)$  is  $\Delta f = f/4$ , and the

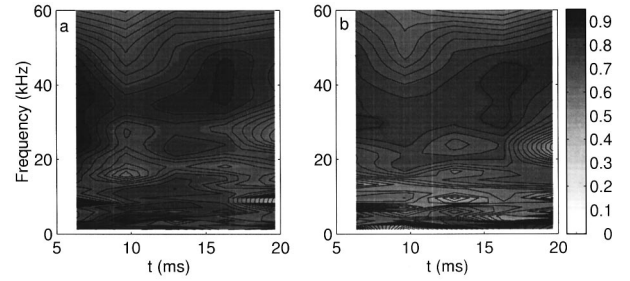


FIG. 6. Time-resolved wavelet coherence versus time of floating potential (a) and ion saturation current fluctuations (b).

time resolution is  $\Delta t = 2a$ . If  $x(t)$  is the signal under analysis, the wavelet transform of  $x(t)$  with respect to a chosen mother wavelet  $\Psi_a(t)$  is defined by<sup>16</sup>

$$W_x(a, \tau) = \int x(t) \Psi_a(t - \tau) dt, \quad (5)$$

where  $a$  is a scaling parameter and  $\tau$  is a time shift parameter. In wavelet analysis time resolution is variable with frequency, so that high frequencies have a sharper time resolution. Wavelet coefficients are averaged over a finite interval  $T: \{T_0 - T/2 \leq \tau \leq T_0 + T/2\}$ .

Similarly to classical Fourier spectral analysis, we defined the cross-power spectrum for two time series  $x(t)$  and  $y(t)$ :

$$C_{yx}(a, T_0) = \int_{T_0} W_x(a, \tau) W_y^*(a, \tau) d\tau. \quad (6)$$

The phase spectrum was obtained from

$$\theta_{yx}(a, T_0) = \tan^{-1} \{ \text{Im}[C_{yx}(a, \tau)] / \text{Re}[C_{yx}(a, \tau)] \}. \quad (7)$$

To quantify where two nonstationary fluctuating signals are linearly correlated at a particular scale (frequency) and time location in a time-scale plane, we defined the coherence spectrum with values in the interval  $0 \leq \gamma_{xy}^2 \leq 1$ . When there is a perfect linear relation at some frequency it is equal to 1. Accordingly, the coherence spectrum was defined as

$$\gamma_{yx}^2(a, T_0) = |C_{yx}(a, T_0)|^2 / C_{xx}(a, T_0) C_{yy}(a, T_0), \quad (8)$$

where  $C_{xx}$  and  $C_{yy}$  are the wavelet autopower spectra of the signals  $x(t)$  and  $y(t)$ , respectively.

The statistical error,  $\varepsilon$ , was determined following Ref. 15 and is given by

$$\varepsilon(\gamma_{yx}) \approx (f_N / fN)^{1/2}, \quad (9)$$

where  $f_N$  is the Nyquist frequency and  $N$  is the number of samples.

Figure 6 shows the temporally resolved coherence between two poloidally separated probes for (a) fluctuating floating potential and (b) ion saturation current. Noise level is  $\varepsilon \approx 0.10$  for low-frequency components. Such spectra are useful to follow the coherence development, in frequency and time, showing alternated regions of high and low coherence values suggesting an intermittent behavior. The coherence is intermittent for both kinds of fluctuations. This electric potential intermittency is not in conflict with the absence of coherent structures (for this fluctuation) previously re-

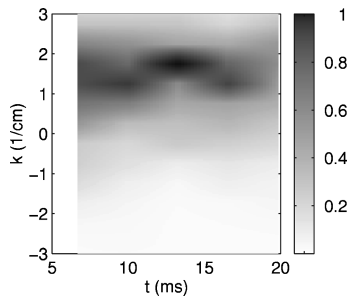


FIG. 7. Time-scale  $S(k)$  wavelet spectrum for ion saturation current fluctuations.

ported, in the average conditional analysis, since the time scale of the wavelet analysis (1 msec) is two orders of magnitude higher than the time scale of the average conditional analysis ( $1 \times 10^{-2}$  msec).

We applied the technique of  $S(k, f)$  spectrum<sup>18</sup> using wavelet auto- and cross-spectra and calculated  $S(f)$  and  $S(k)$  spectra. Figure 7 shows the contour of  $S(k)$  spectrum for ion saturation current fluctuations, suggesting an intermittent wave number variation. This intermittent variation can be seen better in the one-dimensional plot of Fig. 8 that shows the  $S(k=1.3 \text{ cm}^{-1})$  evolution for the spectrum of Fig. 7. The same results are obtained with floating potential fluctuations.

From  $S(k, f)$  we determined the power-weighted average values of poloidal wave vector,  $k_\theta$ , and the phase velocity,  $v_{ph}$ . This was obtained from four pairs of probes at the same radial distance and near the equatorial plane (covering a vertical distance larger than the precision of the vertical plasma column position). Figure 9(a) shows the phase velocity for floating potential fluctuations for pairs of probes at different poloidal positions. These values are comparable to those obtained by using Fourier transforms of data from four similar discharges. Figure 9(b) shows the average values of poloidal-wave-vectors for the same probes. The dispersion is so high that in some discharges the phase velocity and the averaged wave vector values are not well defined for the distant probes above the equatorial plane. There is an asymmetry in the velocity and wave vector, namely, a variation of these quantities for increasing poloidal angles. The observed wave vector variation from the probes below and above the equatorial plane, separated by  $\delta x \approx 1 \text{ cm}$ , is  $\delta k \approx k$ , comparable to the variation expected from calculated dispersion on

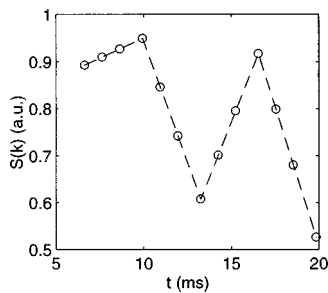


FIG. 8. One-dimensional evolution of the spectrum of Fig. 7 for  $\bar{k} = 1.3 \text{ cm}^{-1}$ .

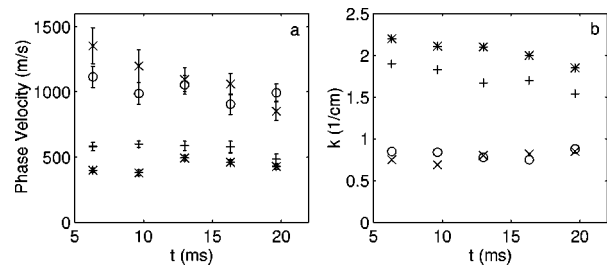


FIG. 9. Wavelet phase velocity, for pairs of probes in different poloidal positions, for floating potential fluctuations (a) and average poloidal wave number for the same probes (b). Symbol (O) for  $\theta \sim -5.6 \times 10^{-2}$  rad, (X) for  $\theta \sim 0$  rad (equatorial plane), (+) for  $\theta \sim 5.6 \times 10^{-2}$  rad, and (\*)  $\theta \sim 1.7 \times 10^{-1}$  rad.

the scale  $k^{-1}$ . This reported behavior is also observed for the phase velocity and wave vectors of ion saturation current fluctuations.

Besides the relevance of the intermittent behavior of the oscillations, relating these quantities to other quantities used in the literature to analyze the turbulent transport would be worthwhile. In fact, spatial and temporal heterogeneity of transport could be used to identify the dominant drive source of particle flux at the scrape-off layer.<sup>1</sup> Therefore, we estimated this transport from the electrostatic fluctuations analyzed in this work. For that, the radial particle flux,  $\Gamma = \langle \tilde{n} \tilde{v} \rangle$ , driven by the density,  $\tilde{n}$ , and plasma potential,  $\tilde{\phi}_p$ , was obtained by calculating the fluctuating radial drift velocity  $\tilde{v} = \tilde{E} / B_t$  ( $\tilde{E} = k \tilde{\phi}_p$ ). In this work we used the spectral analysis to calculate  $\Gamma$  from the equation<sup>1</sup>

$$\Gamma = 2k |C_{n\phi}| \sin(\theta_{n\phi}) / B_t, \tag{10}$$

where, as before,  $B_t$  is the toroidal magnetic field and  $k$  is the plasma potential poloidal wave number. Figure 10 shows the intermittent time resolved frequency transport spectra for probes at the equatorial plane,  $r/a = 1.06$ , maximum value of  $\approx 6 \times 10^{17} \text{ m}^{-2} \text{ s}^{-1} / \text{kHz}$ . Furthermore, the order of magnitude of total particle flux in this radial position was estimated as  $1 \times 10^{19} \text{ m}^{-2} \text{ s}^{-1}$ . This intermittent behavior varies by an order of magnitude during the discharge time. This strong variation was recently predicted by numerical simulations obtained for a model with threshold instability driven by a volumic source, in contrast to a diffusive transport described by a gradient drive mechanism.<sup>19</sup>

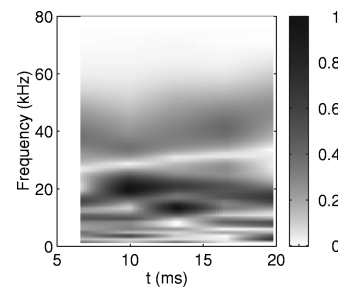


FIG. 10. Intermittent time-resolved frequency transport spectra for probes at the equatorial plane and  $r/a = 1.06$ , maximum value  $\approx 6 \times 10^{17} / \text{m}^2 \cdot \text{s} \cdot \text{kHz}$ .

#### IV. BISPECTRAL WAVELET ANALYSIS

To detect short-lived intermittent coherent structures, we combined wavelet and bispectral analysis by calculating, for short intervals, wavelet bispectra and bicoherences between two frequencies and their sum and difference frequencies. Furthermore, from these wavelet algorithms we obtained evidences of phase coupling between wavelet components of different scale lengths, expected to occur if turbulence presents some structure.<sup>11,15,20</sup>

Bicoherence was calculated according to the following definitions. First, the wavelet bispectrum is

$$B(a_1, a_2) = \int_T W_x^*(a, \tau) W_x(a_1, \tau) W_x(a_2, \tau) d\tau, \quad (11)$$

where  $W_x(a, \tau)$  is the wavelet transform of  $x(t)$  [Eq. (5)] and the integral is taken over a finite interval  $T$  as with the linear-wavelet spectrum. This wavelet-bispectrum measures the amount of phase coupling that occurs between wavelet components of scale lengths  $a_1$ ,  $a_2$ , and  $a$  such that the sum rule  $1/a = 1/a_1 + 1/a_2$  is satisfied. Since the scale lengths may be interpreted as inverse frequencies, the wavelet bispectrum may be interpreted as the coupling of wavelets of frequencies such that  $f = f_1 + f_2$ . Phase coupling is usually expressed by the normalized wavelet bicoherence. Then, substituting the scale lengths by the frequencies we have

$$\begin{aligned} & [b(f_1, f_2)]^2 \\ &= |B(f_1, f_2)|^2 \Big/ \left[ \int_T |W_x(f_1, \tau) W_x(f_2, \tau)|^2 d\tau \right] \\ & \times \left[ \int_T |W_x(f, \tau)|^2 d\tau \right]. \end{aligned} \quad (12)$$

The normalized wavelet-bicoherence is usually plotted over the frequency space  $(f_1, f_2)$  plane. The interaction region includes both sum and difference  $(f_1 \pm f_2)$  interactions. However, due to the symmetry of the interaction, it is sufficient to calculate the bicoherence in the frequency space  $0 < f_1 < f_m$  and  $-f_m < f_2 < f_m/2$ , and, finally, the case  $(f_1, f_2)$  is identical to the case  $(-f_1, -f_2)$ . Here  $f_m$  is the highest frequency admissible for the wavelet ( $f_N/4$ ). This normalized bicoherence takes values between 0 (for a random fluctuation) and 1 (for an unmixed quadratic coupling).

A statistical noise level can be associated to wavelet bicoherence in the same way that Ref. 11:

$$\varepsilon[b(f_1, f_2)] = \{(f_N/n \min(|f_1|, |f_2|, |f|))\}^{1/2}, \quad (13)$$

where  $n$  is the number of points,  $f_N$  is the Nyquist frequency, and  $\min(\dots)$  denotes the minimum frequency of the triplet members; consequently the error is frequency dependent.

To compare cases calculated under the same numerical conditions (wavelet transform and frequency resolution) it is convenient to define the summed bicoherence

$$[b(f)]^2 = [1/s(f)] \sum [b(f_1, f_2)]^2, \quad (14)$$

where the sum is taken over all  $f_1$  and  $f_2$  such that the summation rule is satisfied, and  $s(f)$  is the number of terms of each  $f$ . We can obtain the total bicoherence as

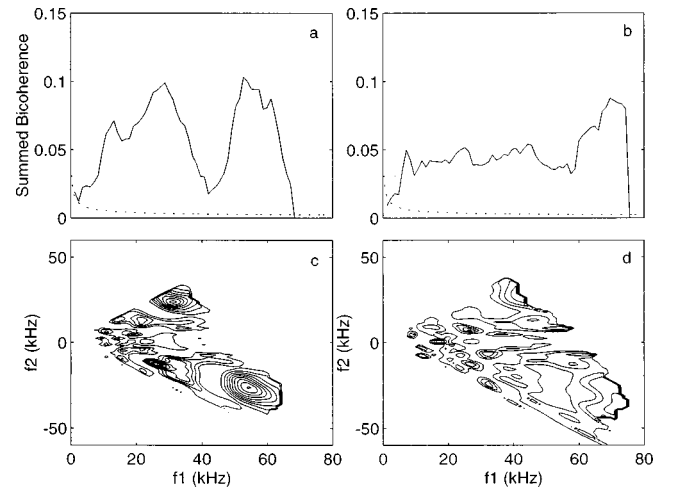


FIG. 11. Summed-autobicoherence for ion saturation current fluctuations for two selected time intervals, 6.3–9.6 ms (a) and 16.2–19.5 ms (b). Dashed lines are the statistical noise level estimates. Contour plots of wavelet bicoherence for the same time intervals and probe (c) and (d).

$$(b)^2 = (1/S) \sum \sum [b(f_1, f_2)]^2, \quad (15)$$

where the sum is taken over all  $f_1$  and  $f_2$ , and  $S$  is the number of terms in the summation. So, the total bicoherence measures the total spectral power of the signal during the interval of the calculated integrals. As wavelet analysis can be done with short data sequences, we can verify the alterations of total bicoherence during a discharge time, identifying intermittent behavior.

It was possible to select in our data five data sections of  $\approx 3.3$  msec to visualize changes in the quadratic coupling between modes during a discharge. Consequently, wavelet bicoherences were calculated with a frequency cell of 1.2 kHz. Figures 11(a) and 11(b) show the summed bicoherence at two selected times (6.3–9.6 and 16.2–19.5 msec) for ion saturation fluctuations, for a probe at fixed poloidal position; at the equatorial plane. Dashed curves are statistical noise level estimates. The value shows the reliability of results. The summed bicoherence shows that the maxima are mainly due to frequencies around 10, 30, and 50 kHz. As turbulent structures are not constant in time, the interval from 16.2–19.5 msec shows a rather low bicoherence. Thus, the cited three peaks show structures that are not clearly present at the last interval. Figures 11(c) and 11(d) show the contour plots of the summed bicoherence for the same intervals. The peaks of the summed bicoherence can be also identified in these plots.

Finally, Fig. 12 shows the total bicoherence versus time for the five data sections of the same probe. Time variation in this plot is a clear indication of turbulent intermittency. The same calculations done for probes at different poloidal positions show similar intermittency. Moreover, the total bicoherence for probes above the equatorial plane, where there could be a density rarefaction,<sup>6,13</sup> shows the highest values. These characteristics are more pronounced for ion saturation current than for floating potential fluctuations.

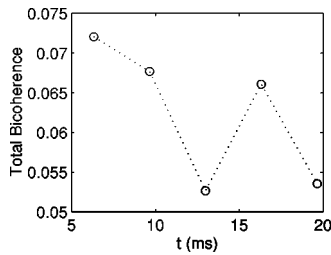


FIG. 12. Total bicoherence versus time for the same probe and data considered in Fig. 8 (maximum statistical error  $\approx 0.01$ ).

## V. CONCLUSIONS

To investigate spatial–temporal characteristics of plasma turbulence in the scrape-off layer, we analyzed electrostatic fluctuations from two probe arrays at the CASTOR tokamak.<sup>6,13</sup>

Using standard statistical analysis, we obtained non-Gaussian probability distribution functions (PDF) for fluctuating ion saturation current, concluding that these fluctuations are not randomly distributed in space and time but associated to coherent structures. Consequently, we applied a conditional averaging analysis<sup>7</sup> to determine a statistical measure of these structures. In fact, we found detectable structures propagating along the poloidal direction with correlation lengths ( $\approx 1$  cm) and lifetimes ( $\approx 10$   $\mu$ sec) larger than the spatial separation ( $\approx 0.5$  cm) and transit time ( $\approx 5$   $\mu$ sec) between two probes. The larger correlation lengths and lifetimes occur at the higher fluctuation amplitude conditions. This is consistent with the hypothesis that coherent structures at large amplitudes would have long lifetimes compared with structures with small conditions. However, for floating potential fluctuations we obtained Gaussian probability distribution functions (PDF). Moreover, in the frequency range of the analysis, the changes in the correlation lengths and lifetimes of these fluctuations were not enough to draw a conclusion about the existence of structures. However, these structures may exist at lower frequencies as observed in turbulence with different spectrum regimes predicted by the turbulence decay laws.<sup>3</sup> Nevertheless, the conditional statistical analysis used cannot always be guaranteed to reveal coherent structures in turbulence. In fact, if many coherent structures are present with randomly distributed velocities, this conditional analysis may fail to show their presence and will overestimate their damping, failing to separate these structures from the background turbulence.

A rough estimate of radial  $E \times B$  drift velocity that causes the particle transport  $\Gamma$  ( $\Gamma \approx \tilde{n} \tilde{E} / B$ ) is  $\tilde{E} / B \approx 1000$  m/sec. With this velocity, the plasma can cross the radial scale length of the SOL of 2.0 cm in 20  $\mu$ sec, which is of the same order of magnitude as the lifetime of the reported  $n$  fluctuation structures. Therefore, these structures can affect the radial particle transport induced by the fluctuating ion saturation and floating potential. Such long life structures were obtained by numerical simulations based on a model of interchange instability (caused by the interaction of the electrostatic sheaths at limiter with  $E \times B$  drifts and diamagnetic

currents due to the curvature and gradient of the magnetic field).<sup>21</sup>

The applied wavelet spectral analysis was very efficient to detect intermittency in the measured electrostatic fluctuations, as observed by the evolution of the coherence and  $S(k)$  spectra in several intervals. In these spectra, we observed a poloidal asymmetry in the fluctuation distribution, namely, the values of phase velocities are lower above the equatorial plane than those obtained at the other positions. This seems to depend on the mode quadratic coupling as discussed in the next paragraph.

The reported turbulence characteristics were used to analyze spatial and temporal heterogeneity of radial particle transport, which varies by an order of magnitude during a discharge. Such a strong variation was recently predicted by numerical simulation based on a threshold instability mechanism, driven by a volumic source as an incoming particle flux from the plasma bulk.<sup>19</sup> The flux predicted by this kind of model is strongly intermittent exhibiting features of self-organized-criticality dynamics.<sup>22</sup> However, although our transport shows a strong intermittency, the available frequency range of our data is not appropriate to identify other characteristics of the proposed dynamics such as avalanche-like bursts and a  $1/f$  decrease of the flux spectrum.<sup>23</sup>

To extract information about relevant nonlinear interactions, we applied wavelet-bicoherence that provides reliable results for short data sequences. So, we found that the evolution of total bicoherence, during different intervals, shows turbulent intermittency in both fluctuations. On the other hand, the quadratic coupling increases with the poloidal angle while the reverse was observed for the phase velocities. This opposite variation, i.e., the tendency of increasing nonlinear behavior to reduce the phase velocity, is expected for drift wave multimode spectra in two-dimensional turbulence.<sup>24</sup>

This work supports the efficacy of wavelet analysis in describing peculiarities of intermittent plasma fluctuations and shows a better detection (compared with Fourier analysis) of turbulence nonlinearity that could be compared with numerical models of turbulence. In fact, previous results obtained with Fourier analysis involved averages in time scales larger than the characteristic time scale of the reported intermittency, preventing its investigation. Eventhough in this analysis turbulence is not described by modes that are constant in time, the physical intuition associated to mode description is still preserved, since a frequency is assigned to each wavelet scale.

In conclusion, by using a conditional analysis, we found evidence of coherent structures related to non-Gaussian behavior of electrostatic fluctuations. These results improve the understanding of the reported intermittency described by the wavelet analysis. Thus, in this sense these complementary techniques are useful to evaluate the significance of turbulence intermittency at the plasma edge.

## ACKNOWLEDGMENTS

The authors thank the referee for suggestions and comments that improved the paper.



This work was partially supported by Brazilian governmental agencies FAPESP (Fundação de Amparo à Pesquisa do Estado de São Paulo) and CNPq (Conselho Nacional de Pesquisa e Desenvolvimento) and by the grant of the Academy of Sciences of the Czech Republic (No. G-IA 1043701).

- <sup>1</sup>J. Wootton, B. A. Carreras, H. Matsumoto, K. McGuire, W. A. Peebles, Ch. P. Ritz, P. W. Terry, and S. J. Zweben, *Phys. Fluids* **2**, 2879 (1990).
- <sup>2</sup>F. Wagner and V. Stroh, *Plasma Phys. Controlled Fusion* **35**, 1321 (1993).
- <sup>3</sup>D. Biskamp, *Nonlinear Magnetohydrodynamics* (Cambridge U.P., Cambridge, 1993).
- <sup>4</sup>S. Benkadda, T. D. Wit, A. Verga, A. Sen, ASDEX Team, and X. Garbet, *Phys. Rev. Lett.* **73**, 3403 (1994).
- <sup>5</sup>B. K. Joseph, R. Jha, P. K. Kaw, S. K. Mattov, C. V. S. Rao, Y. C. Saxena, and Aditya Team, *Phys. Plasmas* **4**, 4292 (1997).
- <sup>6</sup>J. Stockel, I. Duran, V. Dhyani, M. Hron, K. Jakubka, L. Kryska, V. Svoboda, F. Zacek, J. Petrzilka, I. Nanobashvili, and S. Nanobashvili, in *Proceedings of the 1996 International Conference on Plasma Physics*, Nagoya, Japan (International Atomic Energy Agency, Vienna, 1996, Vol. I, p. 322).
- <sup>7</sup>A. V. Filippas, R. D. Bengtson, G. X. Li, M. Meier, Ch. P. Ritz, and E. J. Powers, *Phys. Plasmas* **2**, 839 (1995).
- <sup>8</sup>S. Santoso, E. J. Powers, R. D. Bengtson, and A. Ouroua, *Rev. Sci. Instrum.* **68**, 898 (1997).
- <sup>9</sup>R. M. Castro, M. V. A. P. Heller, I. L. Caldas, Z. A. Brasilio, R. P. da Silva, and I. C. Nascimento, *Phys. Plasmas* **3**, 971 (1996); **4**, 329 (1997).
- <sup>10</sup>B. Ph. van Milligen, C. Hidalgo, and E. Sánchez, *Phys. Rev. Lett.* **74**, 395 (1995).
- <sup>11</sup>B. Ph. van Milligen, E. Sánchez, T. Estrada, C. Hidalgo, B. Brañas, B. Carreras, and L. Garcia, *Phys. Plasmas* **2**, 3017 (1995).
- <sup>12</sup>Ch. P. Ritz, E. J. Powers, and R. D. Bengtson, *Phys. Fluids B* **1**, 153 (1989).
- <sup>13</sup>J. Stockel, V. Dhyani, K. Jakubka, L. Kryska, F. Zacek, I. Duran, M. Horn, and J. Petrzilka, in *Proceedings of the 24th European Physical Society Conference on Controlled Fusion and Plasma Physics*, Berchtesgaden, Germany (European Physical Society, Petit Lancy, 1997, Vol. 21A, p. 625).
- <sup>14</sup>H. L. Pécseli and J. Trulsen, *Phys. Fluids B* **1**, 1616 (1989).
- <sup>15</sup>B. Ph. van Milligen, C. Hidalgo, E. Sánchez, M. A. Pedrosa, R. Balbín, I. García-Cortés, and G. R. Tynan, *Rev. Sci. Instrum.* **68**, 967 (1997).
- <sup>16</sup>C. K. Chui, *An Introduction to Wavelets* (Academic, San Diego, CA, 1992).
- <sup>17</sup>H. Franco, C. Ribeiro, R. P. Silva, I. L. Caldas, and R. M. O. Galvão, *Rev. Sci. Instrum.* **63**, 3710 (1992).
- <sup>18</sup>S. T. Levinson, J. M. Bell, E. J. Powers, and R. D. Bengtson, *Nucl. Fusion* **24**, 527 (1984).
- <sup>19</sup>Y. Sarazin, Ph. Ghendrih, and X. Garbet, in *Proceedings of the 24th European Physical Society Conference on Controlled Fusion and Plasma Physics*, Berchtesgaden, Germany (European Physical Society, Petit-Lancy, 1997), Vol. 21A, p. 193.
- <sup>20</sup>R. A. Moyer, R. D. Lehmer, T. E. Evans, R. W. Conn, and L. Schmitz, *Plasma Phys. Controlled Fusion* **38**, 1273 (1996).
- <sup>21</sup>M. Endler, H. Niedermeyer, L. Giannone, E. Holzhauser, A. Rudyj, G. Theimer, N. Tsois, and ASDEX Team, *Nucl. Fusion* **35**, 1307 (1995).
- <sup>22</sup>P. Beryer, Y. Sarazin, X. Garbet, Ph. Ghendrih, and S. Benkadda, in *Abstracts of the 1998 International Congress on Plasma Physics*, Prague, Czech Republic (International Atomic Energy Agency, Vienna, 1998), P. II, p. 942.
- <sup>23</sup>P. Bak, C. Tang, and K. Wiesenfeld, *Phys. Rev. Lett.* **59**, 381 (1987).
- <sup>24</sup>U. Kauschke and H. Schlueter, *Plasma Phys. Controlled Fusion* **33**, 1309 (1991); **34**, 935 (1992).